

Radio-loud active galaxies in the northern ROSAT All-Sky Survey

I: Radio identifications

S. A. Laurent-Muehleisen¹, R. I. Kollgaard¹, P. J. Ryan¹, E. D. Feigelson¹, W. Brinkmann², and J. Siebert²

¹ Department of Astronomy & Astrophysics, The Pennsylvania State University, University Park, PA, USA 16802

² Max-Planck Institut für Extraterrestrische Physik, D-85740 Garching, Germany

Received date; accepted date

Abstract. We present 5 GHz high resolution VLA observations of 2,127 radio- and X-ray-emitting sources found in both the Green Bank (GB) 5 GHz radio catalog and the ROSAT All-Sky Survey (RASS). We report core flux densities and positions accurate to $\pm 0.5''$. Combined with the GB measurements of the total radio emission, we derive the core-to-lobe ratio of objects in our sample and discuss their core-dominance relative to samples of radio galaxies and BL Lacertae objects. Our results show the RASS/Green Bank (RGB) sample is approximately an order of magnitude more core-dominated than the radio galaxy sample, but is more than an order of magnitude less core-dominated than highly beamed BL Lacertae objects. Using simple beaming models, this indicates the typical object in the RGB catalog exhibits moderately beamed radio emission and is oriented at an angle to the line-of-sight $\bar{\theta}_{\text{RGB}} \sim 25^\circ\text{--}35^\circ$. The case of the origin of the X-ray emission is not as clear; the data are consistent with either an anisotropic unbeamed or moderately beamed X-ray component.

Tables 2 and 3 which present the RGB catalog are available in their entirety only from the CDS via anonymous ftp to cdsarc.u-strasbg.fr (130.79.128.5), via the WWW at <http://cdsweb.u-strasbg.fr/Abstract.html>, or at <ftp://ftp.astro.psu.edu/pub/edf>.

Key words: Surveys – Catalogs – Radio continuum: general – X-rays: general – Radiation mechanisms: non-thermal – Galaxies: active – quasars: general

1. Introduction

The catalog created from the ROSAT All-Sky Survey (RASS) consists of $\sim 60,000$ sources making it the deepest complete sample of soft X-ray (0.07–2.4 keV) sources ever constructed (Voges 1993). Previous X-ray surveys such as the HEAO-1 Large Area Sky Survey (Wood et al. 1984), the Einstein Extended Medium Sensitivity Survey (Gioia et al. 1990; Stocke et al. 1991), and the Einstein Slew Survey (Elvis et al. 1992), consisted of less than 5,000 sources total. Identification programs of these earlier surveys showed the majority of objects are extragalactic consisting mainly of quasars, Seyferts, BL Lacertae objects, clusters of galaxies and occasionally normal galaxies. Similarly, the bulk properties of various samples of optically identified objects in the RASS (e.g. Brinkmann et al. 1994; Brinkmann et al. 1995; Bade et al. 1995) have shown that the RASS contains thousands of extragalactic objects and will therefore provide the largest flux-limited sample of X-ray-emitting AGN for the foreseeable future.

Because RASS positions are known to only $\sim 30''$ accuracy, complete identification of the entire RASS catalog is an enormous task. Correlations with deep surveys at other wavelengths can efficiently create subsamples of manageable size and also select objects of particular interest. We present here 2,127 sources which appear in both the RASS and the 1987 Green Bank (GB) 5 GHz radio survey (Gregory & Condon 1991; Gregory et al. 1996, hereafter called GB96). Because $>70\%$ of the sources in this RASS-Green Bank (RGB) sample are optically unidentified and the positional accuracy of both surveys is low, we obtained high resolution radio observations to enable the identification of unique optical counterparts. Our detection of compact core radio components of these radio-loud active galaxies together with GB observations of the total

radio emission, permits study of the beaming characteristics of these RASS sources. The multiwavelength properties of the previously optically identified sources appear in Brinkmann et al. (1995, B95) and multiband radio observations of a subset are given by Neumann et al. (1994).

This paper is organized as follows: the construction of the RGB catalog is discussed in §2 and the new radio data presented in §3. In §4 we compare our results to the Green Bank data. Section 5 uses simple beaming models to characterize the radio emission of the sources in our catalog and §6 discusses the X-ray beaming properties. The broadband multifrequency properties of the entire RGB catalog, including newly identified optical counterparts and X-ray properties, will be presented in Brinkmann et al. (1996; B96).

2. The RASS-Green Bank (RGB) Sample

Analysis of the Green Bank radio data was performed by fitting single elliptical Gaussian surfaces to local enhancements (Neumann et al. 1994). The final catalog contains $\sim 150,000$ small diameter sources above a detection threshold of 3σ . The flux density limit is ~ 15 mJy in the declination range from $30^\circ - 75^\circ$ and increases to ~ 24 mJy at 0° declination. In order to identify as many radio-emitting objects in the RASS as possible, this list was purposely constructed to be deeper than those lists published later (Becker et al. 1991; Gregory & Condon 1991), which are restricted to $>5\sigma$ sources. The initial radio source catalog is therefore likely to contain many faint spurious sources. The rate of spurious coincidences in the overall RASS-Green Bank correlation ought to be much less, however, since close proximity ($100''$) to a detected X-ray source is required. The 1σ positional accuracy of the Neumann et al. (1994) Green Bank catalog is approximately $\pm 15''$ for bright sources and $\pm 40''$ for fainter ones (Neumann et al. 1994). Direct comparison of the reanalyzed GB flux densities with those published in GB96 shows that for sources >100 mJy the flux densities are accurate to $\sim 20\%$ while for sources <100 mJy the flux densities differ by up to $\sim 40\%$, with the reanalyzed values generally being higher.

The RASS data were processed using the semi-automatic Standard Analysis Software System (SASS; Voges et al. 1992) which determines the sky coordinates and energy of each photon by applying an aspect solution and calibration to each X-ray event. The data are then analyzed using various source detection algorithms, comprising two sliding window techniques and a maximum-likelihood method. Further details are given in Voges (1993).

The RASS and GB surveys were cross-correlated producing a catalog of 2,127 sources with separations of $<100''$. These sources are listed in Tables 2-4 below. The distribution of the separations is well represented by a Gaussian with $\sigma \sim 17''$ for distances up to $40''$ and is ap-

proximately constant beyond this (Figure 1, B95). Because of the highly non-Gaussian nature of the distribution, sources with RASS/GB separations of up to $100''$ were included in this initial catalog. The number of spurious coincidences is believed to be less than 200 objects (B95). The radio flux densities range from 15 mJy to 60 Jy and the X-ray fluxes range from 8×10^{-14} to 4×10^{-10} erg s $^{-1}$ cm $^{-2}$.

3. New VLA Observations

High resolution observations of the RGB sample were made with the NRAO's Very Large Array¹ (VLA) between October 1992 and September 1995. The observations were recorded with the two standard 50 MHz bandwidth IFs at an effective frequency of 4.885 GHz. Table 1 summarizes the observing parameters including the epoch, array configuration, average exposure time per source and beam size. On October 3, 1992, data were collected while the VLA was in a hybrid A/D configuration. We were able to obtain flux densities and positions for these sources only by using the antennas in the low-resolution D-like configuration which yielded insufficient positional accuracy for unambiguous optical identification. For completeness we list these sources separately but do not consider them part of our well-defined sample. They are excluded from further analysis. The region of the sky covered by the D-configuration observations is approximately defined by $0^{\text{hr}} < \alpha < 15^{\text{hr}}$, $0^\circ < \delta < 40^\circ$ and $15^{\text{hr}} < \alpha < 16^{\text{hr}}$, $0^\circ < \delta < 15^\circ$, although high resolution observations for several objects in this region were obtained.

Table 1. Observing Log

Date			Obs Code	VLA Config	Exp. (min)	Beam ($''$)
Oct	19	1992	a	A	1.0	0.4
May	7	1994	b	AnB	0.8	1.3
Sept	15	1994	c	BnC	3.2	4.0
Sept	28	1995	d	AnB	4.2	1.2
Oct	3	1992	e	D	1.0	29

Except for the September 1995 experiment which used 3C48, absolute flux calibration was set using 3C286 and the flux scale of Baars et al. (1977) as modified in the 15APR92 version of the Astronomical Image Processing System (AIPS). Phase calibrators were observed every few hours during each of the experiments.

Data reduction consisted of making tapered $180'' \times 180''$ CLEANed images and using only the first clean com-

¹ NRAO is operated by Associated Universities, Inc., under cooperative agreement with the National Science Foundation.

ponent to phase self-calibrate the data (equivalent to using a point source model at the location of the strongest radio source). A second untapered map, centered at the location of the peak on the first map, was made and CLEANed. The rms noise was measured in a region excluding all sources on the final map. The position and flux density of all sources whose signal-to-noise ratio exceeded 5 were recorded.

In Table 2 we present the 1861 RGB sources for which radio components were detected. We present only a sample page here; a full copy of the table is available from the CDS via anonymous ftp to cdsarc.u-strasbg.fr (130.79.128.5), via the WWW at <http://cdsweb.u-strasbg.fr/Abstract.html> or at ftp://ftp.astro.psu.edu/pub/edf/rgb_tab2.html and [rgb_tab3.html](ftp://ftp.astro.psu.edu/pub/edf/rgb_tab3.html), or by contacting the authors. The columns in Table 2 give the source name, J2000 radio position, observation code (defined in Table 1), signal-to-noise ratio, corrected 5 GHz core VLA flux density (S_5^{core}), total 5 GHz Green Bank flux density taken from the GB96 catalog or from the re-analysis of the GB survey images (S_5^{tot}), and error of the total flux density if the source appeared in GB96. We refer to individual sources using the catalog prefix “RGB J” (RASS-Green Bank catalog, J2000 epoch positions) and append “A”, “B”, “C”, etc. to denote multiple radio sources found on a particular field.

Table 2. See Table at End of document

In Table 3 we show a typical page of similar information for the 436 sources detected only at low resolution which have been excluded from further analysis. Table 4 lists the 83 fields for which no source with a signal-to-noise ratio greater than 5 was detected. Many of these are faint sources cataloged by Neumann et al. (1994) but not in GB96 which used the stricter criterion for source existence and are probably spurious. The columns list the source name, J2000 Green Bank position, observation code, total GB 5 GHz flux density, and error in the total flux density if the source appeared in GB96. In addition, two RGB sources (RGB J0425+179, RGB J1303+488) were not observed with the VLA, but are part of the complete RGB sample.

Table 3. See Table at End of document

Table 4. See Table at End of document

The last column in the tables indicates the presence of a note which indicates: (1) the source may be spurious or related to a diffuse Galactic object (e.g. a supernova remnant); (2) the core radio flux density is from an observation other than this paper; or (3) the source is more than 3σ from its GB position (§3.2).

3.1. Flux Density Corrections

Instrumental effects degrade the measured flux density for sources far from the field center. While time average smearing is insignificant for our observations, both bandwidth smearing (chromatic aberration) and primary beam degradation are significant for many sources in the RGB catalog. The corrected flux density, S , is given by:

$$S = \frac{S'}{B \cdot P} \quad (1)$$

where S' is the flux density from the final map. The bandwidth smearing correction term, B , and the primary beam correction term, P , are given by (Condon et al. 1996):

$$B = \left[1 + \frac{2 \ln 2}{3} \left(\frac{\Delta\nu \rho}{\nu \Theta_0} \right)^2 \right]^{-\frac{1}{2}} \quad \text{and} \quad (2)$$

$$P = (a_0 + a_1 x + a_2 x^2 + a_3 x^3 + a_4 x^4)^{-1}. \quad (3)$$

Here $\Delta\nu$ is the bandwidth (50 MHz), ν is the observing frequency (4.885 GHz), ρ is the angular distance from the field center, Θ_0 is the restoring beam size (Table 1), $x = (\rho\nu)^2$ (ρ in arcminutes), $a_0=1.003$, $a_1=1.086 \times 10^{-3}$, $a_2=3.30 \times 10^{-6}$, $a_3=-3.609 \times 10^{-9}$ and $a_4=3.305 \times 10^{-12}$.

3.2. Source Parameter Reliability

While the formal uncertainties for our reported flux densities and positions can be defined as a quadratic sum of the squares of several error terms (e.g. Condon et al. 1982; Kollgaard et al. 1994), we found these formal uncertainties underestimated the true uncertainties in the reported source parameters. The biggest sources of error in the RGB catalog are instead due to instrumental and technical effects intrinsic to our snapshot mode. In order to assess the reliability in our measured flux densities and positions, we observed 20 RGB sources at more than one epoch after the main survey was completed and used the same data reduction procedure to obtain core flux densities and positions.

These repeated observations show the reported positions for sources in Table 2 are accurate to $\leq 0.5''$ while those in Table 3 are accurate to $\leq 8''$. The core flux densities of the sources observed at multiple epochs varied significantly, however, with the source intensity varying by as much 80% between epochs separated by as little as 10 days. While some of this variability may be intrinsic to the sources, we believe much of it is due to instrumental causes such as different VLA resolution, the lack of phase calibrators near individual sources, very short observation times, and consequently the small number of visibilities used to image large fields. Our tests show the reported flux densities of sources fainter than ~ 20 mJy are generally accurate to $\sim 50\%$ and the brighter sources accurate to $\sim 20\%$.

4. Comparison of the Green Bank and VLA Source Properties

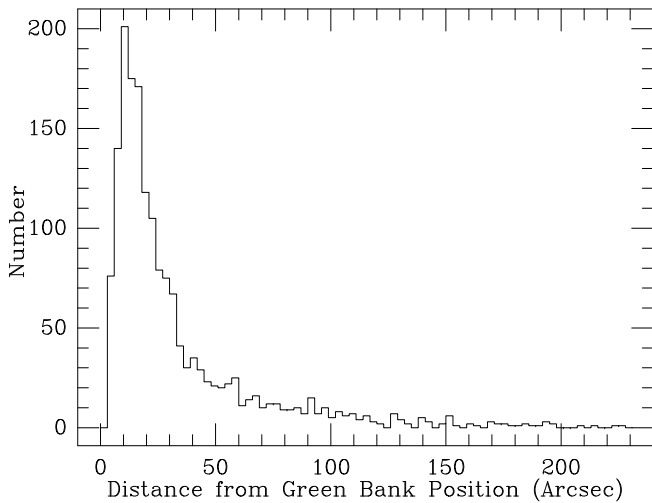


Fig. 1. Distribution of VLA - Green Bank Radio Positions

Figure 1 shows that 82% of the sources are within $\sim 50''$ of the expected GB96 position and the distribution peaks at an offset of $10''$ - $15''$, consistent with the positional errors given in Neumann et al. (1994) and Gregory & Condon (1991). Because the positional uncertainty of the Green Bank positions (which greatly dominate the uncertainties in the VLA positions) are flux dependent, we split the data into two subsets: a bright and faint sample with a division at 75 mJy. We find that the positional accuracies given in Neumann et al. (1994) are then reliable for these two samples. For the analyses that follow, we therefore exclude all bright sources offset from the GB positions by more than $45''$ and all faint sources offset by more than $120''$. These criteria exclude 74 objects from the bright sample and 47 objects from the faint. The number of spurious coincidences which remain in the ta-

bles is quite small with only ~ 31 of the 757 remaining faint sources and ~ 10 of the 813 remaining bright sources expected to be spurious. Flags are given in Table 2 to indicate the sources we excluded.

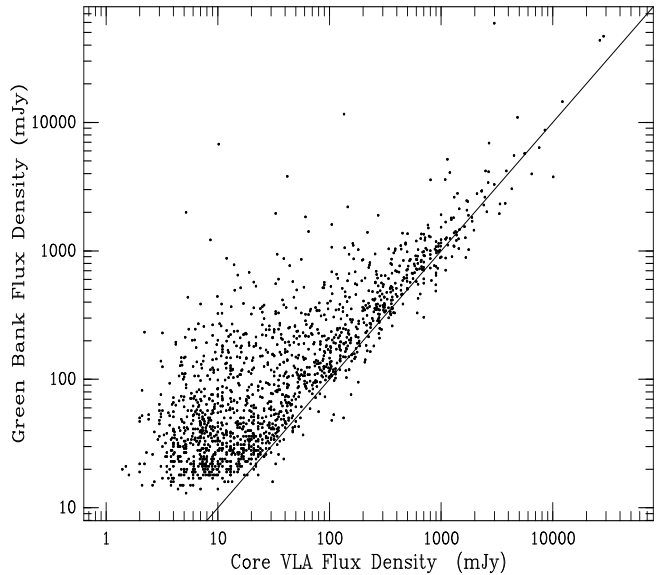


Fig. 2. Log-Log Diagram of the Core VLA Radio Flux Density (mJy) vs. Green Bank Flux Density (mJy) at 5 GHz

Figure 2 shows the flux-flux diagram comparing the core VLA flux density with the Green Bank measurement. For those $\sim 10\%$ of the fields for which more than one source was detected, we have chosen as the “core” component that source which is closest to the RASS position. We also considered using the brightest source on the field or the source closest to the GB position. In all the following analyses, the differences between the results obtained using these three different criterion are well within the uncertainties in the data. Only when we completely excluded the fields with more than one detected source did any of the results change significantly, increasing the median core-to-lobe parameter (§5) by $\sim 20\%$. While source variability and uncertainties in both flux density measurements produces a few points in Figure 2 where $S_5^{\text{VLA}} > S_5^{\text{GB}}$, it is clear that nearly all of the sources in the GB catalog contain emission which is significantly resolved at the arcsecond-scale.

5. Radio Beaming

The radio core-to-lobe ratio, $R = S_5^{\text{core}} / S_5^{\text{lobe}}$, is often used in studies of radio-loud AGN as a relative measure of orientation (e.g. Orr & Browne, 1982). In the absence of high quality interferometric maps showing full details of the radio structure, this ratio can be approximated as $R' = S_5^{\text{VLA}} / (S_5^{\text{GB}} - S_5^{\text{VLA}})$. The distribution of R' (Figure 3a) will differ in detail from that of the true R , both be-

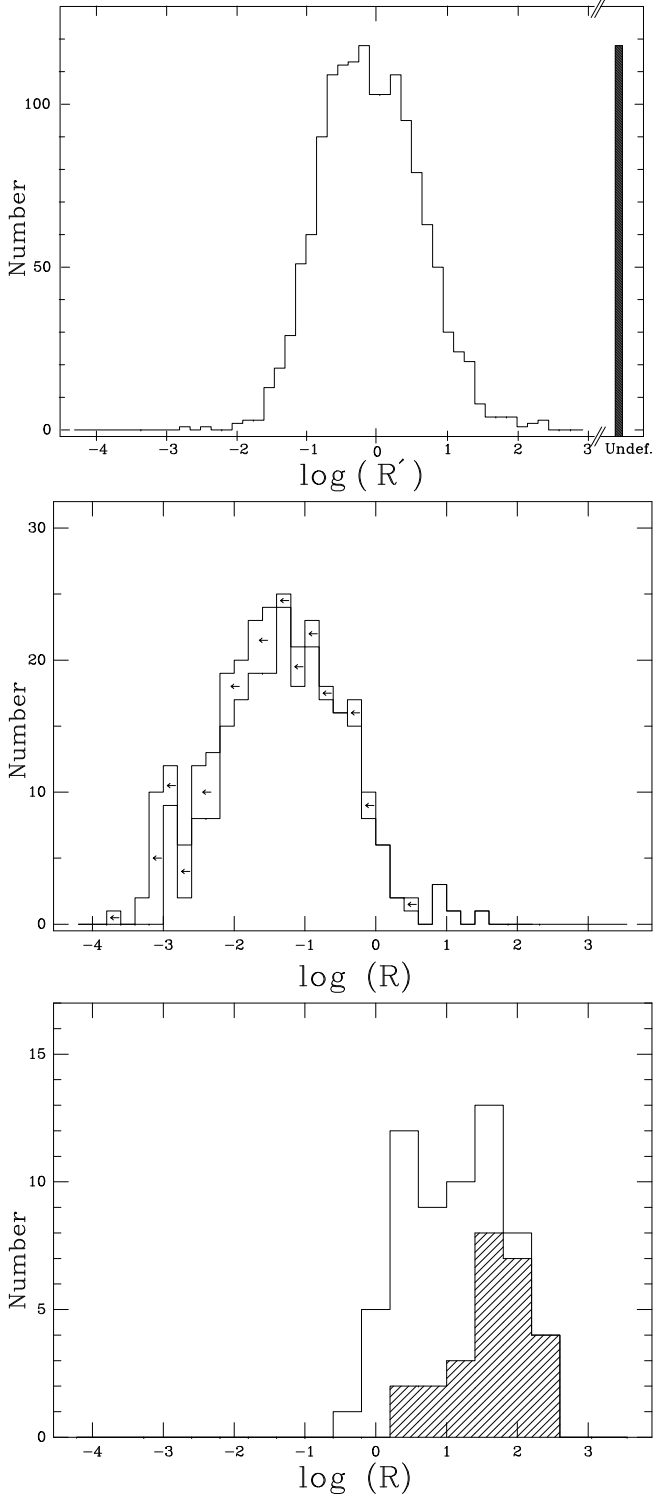


Fig. 3. **a.** Distribution of R' , defined as the (VLA Core Flux Density)/(Green Bank Flux Density - VLA Core Flux Density). This parameter is a rough measure of the radio core-to-lobe ratio. The last bin contains the 118 sources for which the Green Bank flux density is less than the VLA core flux density. **b.** Distribution of the core-to-lobe ratio for radio galaxies. Bins containing undetected cores are denoted with a left-facing arrow. **c.** Distribution of the core-to-lobe ratio for BL Lacertae objects. The hatched histogram distinguishes the radio-selected from the X-ray-selected objects.

cause the VLA and GB observations were not simultaneous and because the low resolution GB measurement may contain some emission from unrelated sources. Nevertheless, we believe these effects should not introduce any significant biases into the distribution of R' .

For comparison we show in Figure 3b the distribution of core-to-lobe ratios for a large sample of FRI and FRII radio galaxies compiled by Zirbel & Baum (1995). (See Zirbel & Baum 1995 for a discussion of the assumptions used to derive R and the upper limits on R for those sources without a measured radio core.) To illustrate the properties of an extremely core-dominated population, we show in Figure 3c the core-to-lobe ratio for BL Lacertae objects, with the radio-selected objects (RBLs) represented by the hatched histogram. The objects shown are the X-ray-selected BL Lacs (XBLs) from the HEAO-1 Large Area Sky Survey (Kollgaard et al. 1996) and the Einstein Extended Medium Sensitivity Survey (Morris et al. 1991), and the radio-selected BL Lacs in the 1 Jansky sample (Stickel et al. 1991). The radio flux densities used to derive the core-to-lobe ratios were taken from Kollgaard et al.

Figure 3 shows the RGB sample is more core-dominated (40% of the sources have $\log R' > 0$) than the radio galaxy sample of Zirbel & Baum (1995; 3% with $\log R > 0$), but is less core-dominated than the BL Lacertae objects (82% with $\log R > 0$). We used the Astronomy SURVival (ASURV) data analysis software (Rev. 1.2; LaValley et al., 1992) to compute the Kaplan-Meier estimator of the R distributions. This properly takes into account the upper limits in the radio galaxy sample (Feigelson & Nelson 1985). The median R of each distribution is given in Table 5. We find that both classes of BL Lac objects are significantly more core-dominated than the RGB sample. The median of the radio galaxy sample, however, is 27 times less core-dominated than the RGB sources.

The differences discussed above are clearly due to the type of object which dominates each of the samples. Although $>70\%$ of the RGB catalog is optically unidentified, most of the identified sources are quasars (B95). A comparison of the optically identified and unidentified sources shows that while the identified sources generally exhibit higher radio and X-ray fluxes, other properties (e.g. their optical colors) are not statistically different (B96). This suggests the unidentified sources are also primarily quasars. The differences in the distribution of R therefore indicate the RGB catalog consists primarily of quasars whose radio emission is moderately beamed.

Within the framework of the unified scheme scenario which hypothesizes flat and steep spectrum quasars are radio galaxies seen close to the line-of-sight (e.g. Barthel 1989), we use a simple beaming model and the core-to-lobe ratio distributions to constrain the jet speed and orientation characteristic of objects in the RGB sam-

ple. The dependence of R on jet speed and orientation are given by (e.g. Urry & Padovani 1995):

$$R \equiv \frac{S_r^{\text{core}}}{S_r^{\text{lobe}}} = f \delta^p \quad (4)$$

where f is the intrinsic core-to-lobe ratio, p is the beaming index, and δ is the Doppler factor:

$$\delta = [\Gamma(1 - \beta \cos \theta)]^{-1}. \quad (5)$$

Here $\beta = v/c$, where v is the bulk velocity, $\Gamma = (1 - \beta^2)^{-\frac{1}{2}}$, and θ is the angle to the line-of-sight. We assume $p = 2.7$, applicable to a jet consisting of a single sphere with a spectral index $\alpha = 0.3$ ($S_\nu \propto \nu^\alpha$; e.g. Pearson & Zensus 1987). We make the further assumption that the Zirbel & Baum (1995) sample of FRI and FRII radio galaxies is characteristic of the parent population of RGB sources, although we examine this hypothesis more carefully at the end of this section.

Table 5. Median Core-to-lobe Ratios

Sample	R
Radio Galaxies	0.019
RGB Sample	0.52
XBLs	1.8
RBLs	20.

Kollgaard et al. (1996), analyzing the same population of radio galaxies and BL Lacertae objects, found that the relative core enhancement of these populations implied that $\Gamma > 4.5$ and probably exceeded $\Gamma = 6$. We therefore assume initially $\Gamma = 6$ for all three populations and adopt $\bar{\theta} = 60^\circ$ for the radio galaxies. (See Kollgaard et al.) For a sample like the RGB catalog which consists largely of radio-loud quasars (B95; B96; Laurent-Muehleisen et al., in preparation), the assumption $\Gamma = 6$ is a reasonable lower limit to the jet speed (Urry & Padovani 1995). Using these assumptions and the median R values in Table 5, this implies that the average angle to the line-of-sight for the RGB sample ($\bar{\theta}_{\text{RGB}}$) is approximately 30° , significantly larger than that obtained for the BL Lac objects where $\bar{\theta}_{\text{XBL}} \approx 20^\circ$ and $\bar{\theta}_{\text{RBL}} \approx 10^\circ$ (Kollgaard et al. 1996).

The assumption that Γ is a single value is most likely incorrect in detail since a range of jet speeds probably characterizes any given population of objects. Assuming $\bar{\theta}_{\text{gal}} = 60^\circ$ and $\Gamma_{\text{RGB}} = \Gamma_{\text{gal}}$, but allowing both Lorentz factors to vary over the range $2 \leq \Gamma \leq 20$, constrains the average angle to the line-of-sight for the RGB sample to lie within a fairly small range, $20^\circ < \bar{\theta}_{\text{RGB}} < 32^\circ$ (Figure 4). If we further constrain $\Gamma \geq 5$, which is a reasonable minimum

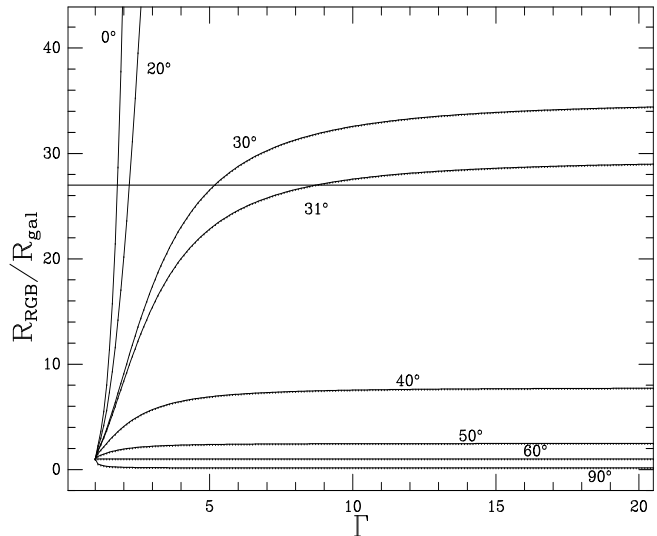


Fig. 4. The predicted line-of-sight orientation for the RGB sample, $\bar{\theta}_{\text{RGB}}$, derived from the relative median core-to-lobe ratios of the RGB and radio galaxy samples. $\bar{\theta}_{\text{gal}} = 60^\circ$ is assumed and the horizontal line is the observed ratio of $\frac{\bar{R}_{\text{RGB}}}{\bar{R}_{\text{gal}}}$.

based on studies of the observed luminosity function of flat and steep spectrum quasars (Urry & Padovani 1995), then $\bar{\theta}_{\text{RGB}}$ is narrowly confined to be about 31° .

Finally, we consider the possibility that the population of FRI and FRII radio galaxies used here is not characteristic of the parent population of objects in the RGB catalog. Assuming some form of a unified scheme is not unreasonable, but it is possible that the RGB sample exhibits an average jet speed substantially different than that characteristic of the Zirbel & Baum (1995) radio galaxy sample. This could be the case if the RGB catalog is biased toward objects with a larger Γ . Using the results of Kollgaard et al. (1996), we fix $\Gamma_{\text{gal}} = 6$ and $\bar{\theta}_{\text{gal}} = 60^\circ$. As before, we constrain Γ_{RGB} to be larger than 5. The average angle to the line-of-sight for the RGB sample is then $20^\circ \leq \bar{\theta}_{\text{RGB}} \leq 35^\circ$. We also consider the case where the intrinsic core-to-lobe ratio (f in Eqn. 4) of the Zirbel & Baum (1995) radio galaxies is different than that of the “true” parent population. Since the RGB catalog is likely dominated by radio- and X-ray-loud quasars, if the FRII-quasar unified scheme is correct (Barthel 1989), the true parent population of RGB objects will have extended radio powers approximately two to three orders of magnitude higher than those objects in Zirbel & Baum (1995). Because the core-to-lobe ratio decreases with increasing extended radio power (Kollgaard et al. 1996), our ratio of the core-to-lobe parameters would be too low by a factor of ~ 4 . However, the effect on the average angle to the line-of-sight is fairly modest, decreasing it to $\bar{\theta}_{\text{RGB}} \sim 25^\circ$. These considerations indicate that $\bar{\theta}_{\text{RGB}}$ is relatively insensitive to assumptions about the detailed characteristics of the parent population.

6. X-ray Beaming?

While the radio emission from radio-loud AGN consists of both beamed (core) and unbeamed (extended) components, the origin of the X-ray emission is not as clear. Only recently has the deconvolution of thermal (host galaxy) X-ray emission from nonthermal unresolved emission been possible (e.g. Worrall & Birkinshaw 1994). Although these studies are preliminary and the sample sizes small, it is reasonable to assume the X-ray fluxes for the RGB sample likely consist of a heterogeneous mix of these two components. General trends should nevertheless persist in the data revealing how much, if any, of the X-ray emission is beamed.

Because redshifts are not available for most of the objects in the RGB sample, flux ratios must be used to compensate for distance effects. Specifically, we compare the ratio of the X-ray flux (F_x , in $\text{erg s}^{-1} \text{cm}^{-2}$) to the beamed radio core (S_r^{core} in mJy) and unbeamed extended (S_r^{ext}) components, with the radio core-to-lobe ratio R' (Figure 5). For those sources where our VLA core measurement exceeded the GB total flux density measurement, we derive limits (in both the ordinate and abscissa) by assuming the maximum uncertainty in the radio flux densities, namely 20% error for sources >20 mJy and 50% error otherwise. (See §3.2.) It is likely that the uncertainty in the measurements and not source variability are to blame since most of the sources which suffer from this effect are faint and therefore have the greatest uncertainty in their measured flux densities. Nevertheless, because there are so many sources where $S_r^{\text{ext}} \geq S_r^{\text{core}}$, the statistical significance of the following analyses remains unchanged whether the upper limits are halved or doubled, thus insuring our results are insensitive to our particular method for computing the limits.

Figure 5a shows the ratio of the total X-ray flux to extended radio flux density (F_x/S_r^{ext}) versus R' while in Figure 5b we show the ratio of the total X-ray flux to core radio flux density (F_x/S_r^{core}) versus R' . Two trends are seen in Figure 5: F_x/S_r^{ext} increases with increasing R' , and F_x/S_r^{core} decreases with increasing R' . Both these trends are statistically significant at the $>99.99\%$ level. Two possible biases could affect the correlations. First, if the 83 sources for which no arcsecond-scale source was detected (Table 4) are real and not spurious detections in the 3σ Green Bank catalog, they must be lobe-dominated and would appear on the left-hand side of Figure 5a. If these sources were also systematically X-ray brighter so that they had high F_x/S_r^{ext} ratios then they could populate the upper left portion of Figure 5a; however, the ROSAT fluxes for these sources span the same range as the detected sources, indicating this potential bias is not present. Second, the different flux limits of the original GB catalog ($S_r^{\text{tot}} \geq 15$ mJy) and the deeper VLA core measurements (~ 1 mJy) imply core-dominated sources with $1 \leq S_r^{\text{tot}} \leq 15$ mJy are missing from the RGB catalog. These

“missing” sources could destroy the correlation in Figure 5b only if their core-to-lobe ratios exceeded ~ 10.0 and F_x exceeded $\sim 10^{-13} \text{ erg s}^{-1} \text{cm}^{-2}$. This is not the case, however, since our VLA flux limit is only one order of magnitude deeper than the GB flux limit thereby constraining the core-to-lobe ratios of the missing sources to be $-1.0 < \log R' < 1.0$. We therefore conclude that the two trends in Figure 5 are real.

To understand these relationships, we characterize the X-ray emission by an X-ray “core-to-extended” ratio, R_X , defined by:

$$R_X \equiv \frac{F_x^{\text{core}}}{F_x^{\text{ext}}}, \quad (6)$$

If the X-ray core beaming is simply related to the radio core beaming, we can write $R_X = kR'$ where k is a constant. The quantities plotted in Figure 5 are then:

$$\frac{F_x}{S_r^{\text{core}}} = \frac{F_x^{\text{ext}}}{S_r^{\text{ext}}} \frac{1 + kR'}{R'} \quad (7)$$

and

$$\frac{F_x}{S_r^{\text{ext}}} = \frac{F_x^{\text{ext}}}{S_r^{\text{ext}}} (1 + kR'). \quad (8)$$

First we consider the case where the X-ray emission is isotropic so that $F_x = F_x^{\text{ext}}$ and $k=0$. Then as the angle to the line-of-sight decreases, both R' and S_r^{core} increase but F_x remains constant. The ratio of F_x/S_r^{core} would therefore be anticorrelated with R' as seen in Figure 5b. However, the ratio of F_x/S_r^{ext} would be uncorrelated with R' since neither parameter would vary with orientation. The positive correlation in Figure 5a, therefore rules out the possibility that X-ray emission for sources in the RGB catalog is entirely isotropic.

If we now consider the other extreme where the X-ray emission consists of a much higher fraction of beamed radiation than the radio emission ($k \gg 1$). F_x/S_r^{ext} should then be correlated with R' , as observed, but the ratio of F_x/S_r^{core} would become uncorrelated with R' at even modest values of R' , which is clearly not seen (Figure 5b). Therefore, if the X-ray emission is beamed, it is not characterized by a high k -value. As an alternative to the models presented in Equations 6-8, we consider the case where $\Gamma_x \neq \Gamma_r$. Such a scenario has been proposed in terms of an accelerating jet model for BL Lac objects (e.g. Ghisellini & Maraschi 1989) where $\Gamma_x \leq \Gamma_r$. We find that in order to produce the relations seen in Figure 5 which are valid over three orders of magnitude in the X-ray to radio flux ratios and five orders of magnitude in R' , $\Gamma_x \geq 4$ and $\Gamma_r \geq 6$, which is consistent with bulk velocities inferred through other means (e.g. Urry & Padovani 1995).

Figures 5a and 5b therefore indicate the X-ray emission of the RGB sample is neither entirely isotropic ($R_X=0$) nor characterized by a high k -value. However, the scatter in the diagrams is large enough to prevent an accurate

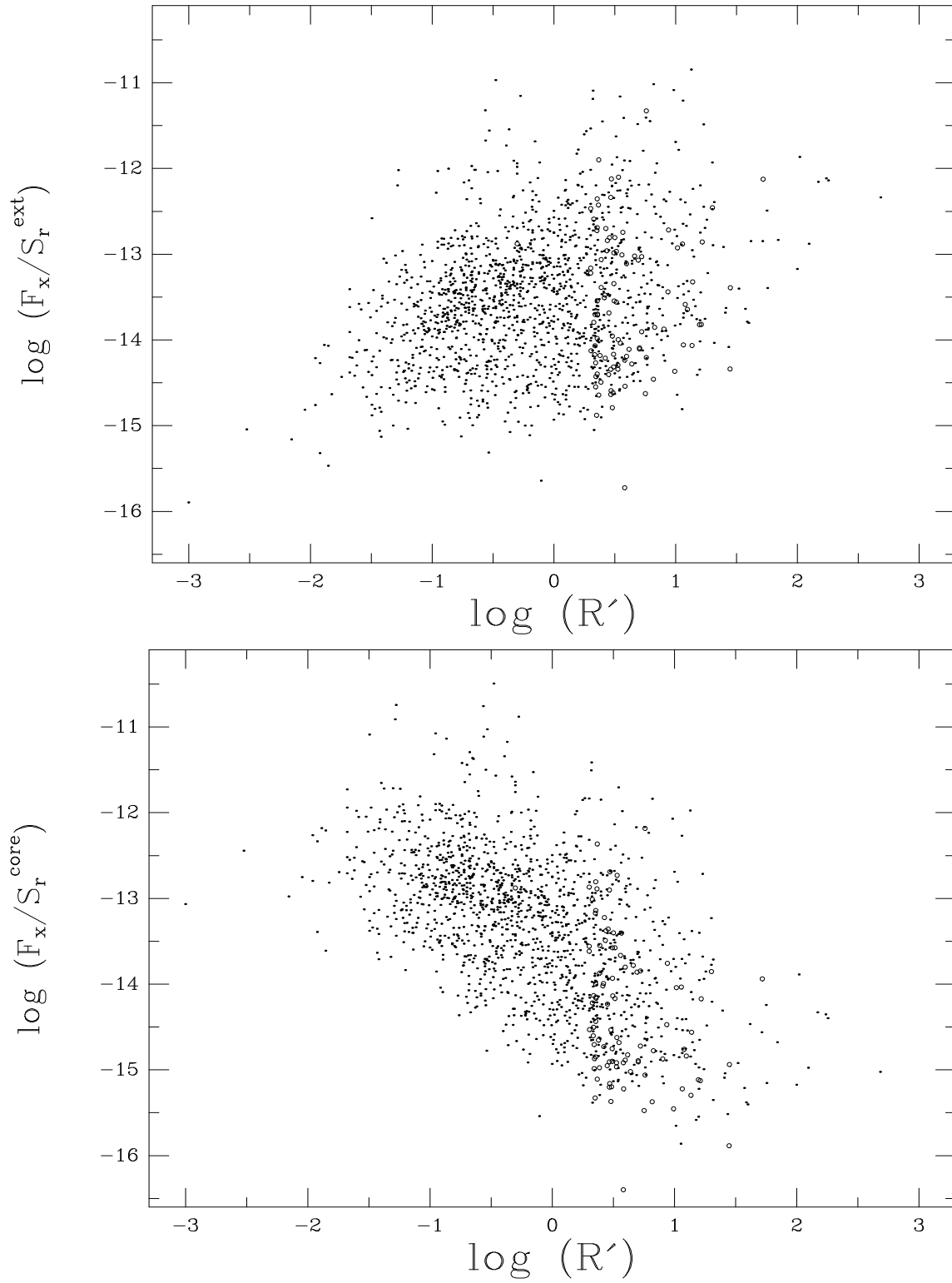


Fig. 5. a. The ratio of X-ray to extended radio flux density as a function of the radio core-to-lobe ratio, R' , for the RGB sources. For those 118 sources for which the VLA core flux density was greater than the Green Bank total flux density, we derive upper limits as described in the text. These points are denoted by open circles in the diagram. **b.** Similar to (a) except the ordinate shows the ratio of X-ray to core radio flux density.

measurement of the fraction of beamed X-rays or even to distinguish beamed X-ray emission from unbeamed but anisotropic emission. The latter could arise, for example, from a population of objects with an obscuring torus with varying column density which blocks more soft X-rays as the torus becomes more edge-on to the line-of-sight.

The large scatter in the diagrams is primarily due to the heterogeneity of the RGB sample, which includes radio galaxies, quasars and BL Lacs. Examination of a single class of AGN, such as RGB BL Lacs, can yield more quantitative results (Laurent-Muehleisen et al., in preparation).

7. Conclusions

We present subarcsecond radio positions and core radio flux densities for all 2,127 sources appearing in both the Green Bank 5 GHz and in the ROSAT All-Sky Survey catalogs. The accuracy of the positions is sufficient to give unique optical identifications for the X-ray- and radio-emitting sources (B96).

This RGB sample is comprised principally of radio-loud AGN. It is complete and unbiased with well-defined selection criteria: X-ray flux above the RASS sensitivity limit (which depends only on ecliptic latitude), arcminute-scale radio flux density above $\simeq 15$ mJy at 5 GHz, and declination between 0° and 75° .

The radio emission of the RGB sample is found to be more core-dominated than ordinary radio galaxies but less than strongly beamed BL Lac objects, which suggests it consists primarily of moderately beamed AGN. Using simple beaming models, the typical RGB object is shown to be dominated by a jet oriented at an intermediate angle to the line-of-sight ($\bar{\theta}_{\text{RGB}} \sim 25^\circ$ – 35°). The X-ray beaming properties are not tightly constrained, but exclude the extremes of purely isotropic emission and of X-ray emission which consists of a significantly higher fraction of beamed flux than is characteristic of the radio emission.

Acknowledgements. We wish to thank C. Palma for help with the data reduction at Penn State. This work was partially supported by NASA under Grant NAGW-2120. We have made use of the NASA/IPAC Extragalactic Database, operated by the Jet Propulsion Laboratory, California Institute of Technology, under contract with NASA.

References

- Baars, J. W. M., Gnezel, R., Pauliny-Toth, I. I. K. & Witzel, A. 1977, *A&A*, 61, 99
- Bade, N., Fink, H. H., Engels, D., Voges, W., Hagen, H. J., Wisotzki, L. & Reimers, D., 1995, *A&AS*, 110, 469
- Barthel, P. D., 1989, *ApJ*, 336, 606
- Baum, S. A. & Heckman, T., 1989, *ApJ*, 336, 681
- Becker, R. H., White, R. L. & Edwards, A. L., 1991, *ApJS*, 75, 1
- Brinkmann, W., Siebert, J. & Boller, Th., 1994, *A&A*, 281, 355
- Brinkmann, W., Siebert, J., Reich, W., Fürst, E., Reich, P., Voges, W., Trümper, J. & Wielebinski, R., 1995, *A&AS*, 109, 147 (B95)
- Brinkmann, W., Siebert, J., Feigelson, E. D., Kollgaard, R. I., Laurent-Muehleisen, S. A. & McMahon, R., 1996, (in preparation; B96)
- Browne, I. W. A. & Murphy, V., 1987, *MNRAS*, 226, 601
- Burns, J. O., Basart, J. P., De Young, D. S. & Ghiglia, D. C., 1984, *ApJ*, 283, 515
- Condon, J. J., Condon, M. A. & Hazard, C. 1982, *AJ*, 87, 739
- Condon, J. J., Cotton, W. D., Greisen, E. W., Yin, Q. F., Perley, R. A. & Broderick, J. J., 1996, *AJ*, in preparation
- Elvis, M., Plummer, D., Schachter, J. & Fabbiano, G., 1992, *ApJS*, 80, 257
- Feigelson, E. D., Isobe, T. & Kembhavi, A., 1984, *AJ*, 89, 1464
- Feigelson, E. D. & Nelson, P. I., 1985, *ApJ*, 293, 192
- Ghisellini, G. & Maraschi, L., 1989, *ApJ*, 340, 181
- Ghisellini, G., Padovani, P., Celotti, A., Maraschi, L., 1993, *ApJ*, 407, 65
- Gioia, I., Maccacaro, T., Schild, R., Wolter, A., Stocke, J., Morris, S. & Henry, J. P., 1990, *ApJS*, 72, 567
- Gower, A. C. & Hutchings, A. C., 1984, *AJ*, 89, 1658
- Gregory, P. C. & Condon, J. J. 1991, *ApJS*, 75, 1011
- Gregory, P. C., Scott, W. K., Douglas, K. & Condon, J. J. 1996, *ApJS*, submitted (GB96)
- Hintzen, P., Ulvestad, J. & Owen, F., 1983, *AJ*, 88, 709
- Hutchings, J. B., Price, R. & Gower, A. C., 1988, *ApJ*, 329, 122
- Kellerman, K. I., Sramek, R. A., Schmidt, M., Shaffer, D. B. & Green, R. F., 1989, *AJ*, 98, 1195
- Kollgaard, R. I., Wardle, J. F. C., Roberts, D. H. & Gabuzda, D. C., 1992, *AJ*, 104, 1687
- Kollgaard, R. I., Brinkmann, W., Chester, M. M., Feigelson, E. D., Hertz, P., Reich, P. & Wielebinski, R., 1994, *ApJS*, 93, 145
- Kollgaard, R. I., Palma, C., Laurent-Muehleisen, S. A., Feigelson, E. D., 1996, *ApJ*, To Appear
- Laurent-Muehleisen, S. A., Kollgaard, R. I., Ciardullo, R. B., Feigelson, E. D., 1996, in preparation
- Lawson, A. J., Turner, M. J. L., Williams, O. R., Stewart, G. C., Saxton, R. D., 1992, *MNRAS*, 259, 743
- LaValley, M., Isobe, T. & Feigelson, E. D., 1992, *BAAS*, 24, 839
- Linfield, R. & Perley, R., 1984, *ApJ*, 279, 60
- Miller, P., Rawlings, S. & Sanders, R., 1993, *MNRAS*, 263, 425
- Morris, S. L., Stocke, J. T., Gioia, I. M., Schild, R. E., Wolter, A., Maccacaro, T. & Della Ceca, R., 1991, *ApJ*, 380, 49
- Murphy, D. W., Browne, I. W. A. & Perley, R. A., 1993, *MNRAS*, 264, 298
- Neumann, M., Reich, W., Fürst, E., Brinkmann, W., Reich, P., Siebert, J., Wielebinski, R. & Trümper, J., 1994, *A&AS*, 106, 303
- O'Dea, C. P. & Owen, F. N., 1985, *AJ*, 90, 927
- Orr, M. J. & Browne, I. W. A., 1982, *MNRAS*, 200, 1067
- Pearson, T. J. & Zensus, J. A., 1987, in *Superluminal Radio Sources*, Ed. J. A. Zensus & T. J. Pearson (Cambridge University Press, Cambridge), 1
- Perley, R. A., 1982, *AJ*, 87, 859
- Punsly, B., 1995, *AJ*, 109, 1555

- Stickel, M., Padovani, P., Urry, D. M., Fried, J. W. & Kühr, H., 1991, ApJ, 374, 431
- Stocke, J. T., Morris, S. L., Gioia, I. M., Maccacaro, T., Schild, R., Wolter, A., Fleming, T. A. & Henry, J. P., 1991, ApJS, 76, 813
- Ulvestad, J. S. & Wilson, A. S., 1984, ApJ, 278, 544
- Urry, C. M. & Padovani, P., 1995, PASP, 107, 803
- Voges, W., Gruber, R., Paul, J., Bickert, K., Bohnet, A., Bur-sik, J., Dennerl, K., Englhauser, J., Hartner, G., Jennert, W., Köhler, H. & Rosso, C., 1992, The ROSAT Standard Analysis Software System, ESA ISY-3, p. 223
- Voges, W., 1993, Adv. Space Res., Vol. 13, No. 12, 391
- Wood, K. S., et al., 1984, ApJS, 56 507
- Worrall, D. M. & Birkinshaw, M., 1994, ApJ, 427, 134
- Wrobel, J. M. & Heeschen, D. S., 1984, ApJ, 287, 41
- Zirbel, E. L. & Baum, S. A., 1995, ApJ, 448, 521

This article was processed by the author using Springer-Verlag
 \LaTeX A&A style file *L-AA* version 3.

Notes to Table 2

- 1545+646A: More than 3σ from GB position
- 1545+646B: More than 3σ from GB position
- 1547+208: Core radio flux from Miller et al. 1993
- 1549+026: Core radio flux from Murphy et al. 1993
- 1550+113: Core radio flux from Hintzen et al. 1983
- 1604+012: Core radio flux from Baum & Heckman 1989
- 1608+104: Core radio flux from Murphy et al. 1993
- 1609+179: Core radio flux from Hutchings et al. 1988
- 1617+350: More than 3σ from GB position
- 1620+176: Core radio flux from Hintzen et al. 1983
- 1625+268: Core radio flux from Feigelson et al. 1984

Notes to Table 3

- 0242+083: More than 3σ from GB position

Notes to Table 4

- 0140+087: Possibly Spurious Source; See Condon et al. 1994
- 0205+648: Extended Source
- 0247+187: Extended Source
- 0317+415: Confused Field - Possibly Spurious Source
- 0528+344: Extended Source
- 0533+210: Confused Field - Possibly Spurious Source
- 0535+222: Confused Field - Possibly Spurious Source
- 0641+080: Extended Source
- 1232+123: Confused Field - Possibly Spurious Source
- 1728+086: Confused Field - Possibly Spurious Source
- 1852+006: Extended Source (known SNR)
- 1859+071: Confused Field or Extended Source
- 2015+386: Confused Field - Possibly Spurious Source
- 2212+589: Extended Source
- 2302+587: Extended Source
- 2323+584: Confused Field - Possibly Spurious Source

Table 2^a Radio Source Properties (Sample Page)

Name	α (J2000) h m s	δ ° ' "	Obs	S/N	S_5^{core} (mJy)	S_5^{tot} (mJy)	ΔS_5^{tot} (mJy)	Notes
1542+496	15 42 32.04	49 38 42.6	a	64	25	34	4	
1542+614	15 42 56.94	61 29 55.3	b	106	102	121	11	
1543+048	15 43 33.92	04 52 19.2	b	87	154	293	26	
1544+041	15 44 59.43	04 07 46.3	b	111	358	387	34	
1545+348	15 45 10.95	34 52 46.8	a	11	7	27	4	
1545+646A	15 45 15.11	64 39 23.2	a	19	17	75	7	*
1545+646B	15 45 16.44	64 39 19.9	a	30	26	75	7	*
1545+534	15 45 35.51	53 24 21.4	a	12	4	49	5	
1547+208	15 47 43.53	20 52 16.7	39	870	77	*
1548+351	15 48 17.92	35 11 28.2	b	92	60	107	10	
1548+582	15 48 25.72	58 13 17.6	b	21	9	186	17	
1548+698	15 48 38.53	69 49 19.6	b	38	28	135	12	
1549+506	15 49 17.47	50 38 05.8	c	4133	934	731	65	
1549+026	15 49 29.43	02 37 01.2	1147	1111	99	*
1550+390	15 50 39.49	39 05 09.8	a	13	7	28	...	
1550+113	15 50 43.60	11 20 46.9	176	543	48	*
1551+581	15 51 58.22	58 06 44.5	b	205	263	348	31	
1552+653	15 52 08.92	65 18 10.4	a	16	9	20	4	
1552+705	15 52 52.22	70 32 28.1	c	44	7	25	4	
1553+140	15 53 06.19	14 00 58.6	b	43	21	123	11	
1554+201	15 54 24.13	20 11 25.4	a	54	20	51	6	
1555+111	15 55 43.05	11 11 24.4	b	90	398	510	45	
1556+244	15 56 03.91	24 26 52.9	b	134	56	109	10	
1557+278	15 57 09.07	27 48 37.6	b	25	5	29	4	
1557+354	15 57 41.65	35 29 51.5	b	37	13	80	8	
1557+215	15 57 44.91	21 31 51.5	a	12	4	32	5	
1558+626	15 58 14.58	62 38 52.5	a	35	15	45	5	
1558+201	15 58 37.09	20 09 23.6	a	44	12	32	5	
1600+332A	16 00 50.75	33 12 09.1	b	13	3	32	5	
1600+332B	16 00 51.13	33 12 06.8	b	21	4	32	5	
1601+539	16 01 28.27	53 56 50.9	c	50	8	43	...	
1601+179	16 01 51.56	17 54 09.9	a	23	7	74	7	
1602+308	16 02 18.04	30 51 09.3	a	35	20	24	4	
1602+267	16 02 39.63	26 46 06.0	b	95	100	117	11	
1602+422	16 02 58.85	42 12 03.3	a	19	6	31	...	
1603+090A	16 03 17.19	09 00 42.0	b	32	10	99	10	
1603+090B	16 03 17.91	09 00 37.9	b	20	7	99	10	
1603+731	16 03 46.92	73 08 42.6	c	52	8	41	...	
1603+575	16 03 55.93	57 30 54.3	b	110	265	365	32	
1604+572	16 04 37.36	57 14 36.7	b	103	384	329	29	
1604+012	16 04 45.35	01 17 51.0	65	1415	126	*
1604+239A	16 04 56.47	23 55 59.8	b	19	7	193	17	
1604+239B	16 04 56.89	23 55 54.3	b	10	4	193	17	
1605+177	16 05 08.99	17 43 47.5	b	13	7	386	34	
1605+379	16 05 15.52	37 56 43.9	b	201	55	50	6	
1605+546A	16 05 37.99	54 39 17.4	a	13	6	76	7	
1605+546B	16 05 38.81	54 39 29.9	a	8	3	76	7	
1606+137	16 06 18.39	13 45 32.8	a	48	32	53	6	
1606+540	16 06 23.56	54 05 55.7	b	106	61	89	8	
1606+272	16 06 58.31	27 17 05.6	b	195	147	228	20	
1608+293	16 08 13.78	29 21 26.2	a	39	13	50	...	
1608+079	16 08 18.70	07 54 49.0	b	32	16	109	11	
1608+603A	16 08 19.38	60 18 31.1	a	24	16	59	6	
1608+603B	16 08 20.55	60 18 28.2	a	40	26	59	6	
1608+402A	16 08 22.13	40 12 10.8	b	27	12	240	21	
1608+402B	16 08 22.17	40 12 17.9	b	267	122	240	21	
1608+104	16 08 46.20	10 29 07.8	1347	1412	125	*
1609+179	16 09 11.27	17 56 16.3	15	238	21	*
1609+048	16 09 19.87	04 49 40.1	a	14	6	34	6	
1610+671A	16 10 02.61	67 10 29.8	a	10	5	36	5	
1610+671B	16 10 04.07	67 10 26.4	a	27	13	36	5	
1610+671C	16 10 05.95	67 10 21.9	a	7	4	36	5	
1610+728A	16 10 48.12	72 50 50.3	a	12	7	20	4	
1610+728B	16 10 49.94	72 50 46.4	a	9	5	20	4	
1611+622A	16 11 05.77	62 16 31.9	a	19	16	50	5	
1611+622B	16 11 07.09	62 16 28.6	a	10	9	50	5	
1613+342	16 13 41.06	34 12 47.9	b	11817	3366	2324	207	
1616+049	16 16 37.56	04 59 32.8	b	124	711	916	81	
1616+557	16 16 39.46	55 45 26.4	a	18	6	33	4	
1616+363	16 16 55.58	36 21 34.5	b	341	269	286	25	
1617+411	16 17 06.32	41 06 47.0	b	177	81	124	11	
1617+066	16 17 13.49	06 37 29.1	b	22	5	246	22	
1617+552	16 17 16.33	55 15 47.0	a	284	32	58	6	
1617+350	16 17 32.82	35 00 23.9	b	8	5	478	42	*
1618+083A	16 18 25.68	08 20 13.4	b	13	23	119	11	
1618+083B	16 18 26.93	08 19 50.8	b	87	150	119	11	
1618+063	16 18 30.60	06 22 11.3	a	32	17	31	6	
1618+219	16 18 47.93	21 59 25.5	a	13	4	40	5	
1619+305	16 19 02.48	30 30 51.5	a	82	38	44	5	
1620+176	16 20 21.83	17 36 23.9	195	584	52	*
1621+377	16 21 11.30	37 46 05.1	b	96	155	201	18	
1621+427	16 21 31.10	42 45 23.2	b	13	2	39	5	
1622+401	16 22 29.32	40 06 43.7	a	57	30	58	6	
1622+359	16 22 37.67	35 55 40.9	a	23	8	19	4	
1623+379A	16 23 03.10	37 55 17.9	b	10	3	176	16	
1623+379B	16 23 03.13	37 55 20.6	b	56	16	176	16	
1623+664	16 23 04.54	66 24 01.1	b	156	243	481	43	
1623+391	16 23 07.62	39 09 32.5	b	51	292	244	22	
1623+076	16 23 58.25	07 41 30.6	b	132	171	149	14	
1624+374	16 24 43.35	37 26 42.4	a	38	14	31	4	
1625+268	16 25 14.30	26 50 26.6	32	233	21	*
1625+270	16 25 30.69	27 05 46.3	b	73	31	210	19	
1625+583	16 25 58.03	58 20 31.4	a	11	4	15	...	
1626+513	16 26 11.62	51 20 38.3	a	34	14	35	5	
1626+352	16 26 25.83	35 13 41.3	a	40	14	19	4	
1626+581A	16 26 37.25	58 09 17.7	b	215	144	315	28	
1626+526	16 26 37.92	52 38 04.6	a	31	17	27	4	
1626+581B	16 26 38.00	58 09 03.2	b	63	43	315	28	
1627+317	16 27 11.87	31 43 59.2	a	66	38	76	7	
1627+608A	16 27 12.32	60 53 45.9	a	20	10	44	5	

^aTable 2 is available in its entirety in computer-readable format at <http://cdsweb.u-strasbg.fr/Abstract.html> or ftp://ftp.astro.psu.edu/pub/edf/rgb_tab2.html or by contacting the authors.

Table 3^a Radio Source Properties: Low Resolution Data (Sample Page)

Name	α (J2000) h m s	δ ° ' "	S/N	S ₅ ^{core} (mJy)	S ₅ ^{tot} (mJy)	ΔS_5^{tot} (mJy)	Notes
0000+082	00 00 07.2	08 16 47	52	48	52	7	
0002+021	00 02 46.7	02 09 14	29	17	29	...	
0004+117	00 04 58.6	11 42 05	71	27	33	5	
0011+324	00 11 46.8	32 25 49	28	14	28	4	
0015+040	00 15 53.8	04 00 41	25	16	48	7	
0017+084	00 17 41.5	08 27 56	36	32	98	10	
0018+291	00 18 51.2	29 07 45	33	25	44	6	
0022+179	00 22 41.1	17 56 35	26	14	34	5	
0027+261	00 27 27.3	26 07 10	58	60	54	6	
0027+335	00 27 58.0	33 35 18	33	34	81	8	
0028+248	00 28 04.2	24 48 25	29	24	38	5	
0028+310	00 28 12.5	31 03 20	48	44	88	8	
0030+360	00 30 06.2	36 05 39	31	26	29	4	
0030+380	00 30 18.8	38 04 02	47	47	54	6	
0031+302	00 31 22.3	30 16 06	74	76	44	5	
0036+377	00 36 51.6	37 43 49	26	22	24	4	
0039+394	00 39 55.4	39 29 35	57	26	26	4	
0041+379	00 41 23.4	37 59 00	64	49	50	6	
0041+090	00 41 35.3	09 02 06	79	48	57	7	
0042+366	00 42 08.4	36 41 16	25	12	20	...	
0043+244	00 43 52.4	24 24 24	61	34	30	5	
0044+225	00 44 49.9	22 31 20	27	11	17	...	
0044+104	00 44 58.2	10 27 19	41	27	82	8	
0045+253	00 45 13.2	25 22 39	34	20	39	5	
0045+214	00 45 19.6	21 27 43	66	45	49	6	
0045+122	00 45 43.4	12 17 12	113	60	62	7	
0047+033	00 47 06.0	03 19 57	103	37	62	8	
0047+215	00 47 10.5	21 34 18	11	7	31	...	
0049+244	00 49 42.5	24 26 44	33	22	61	6	
0051+044	00 51 59.1	04 27 42	109	68	69	8	
0056+278	00 56 17.8	27 53 53	66	66	89	9	
0101+000	01 01 25.4	00 00 59	8	4	40	...	
0102+133	01 02 35.3	13 22 26	9	5	24	...	*
0104+261	01 04 13.8	26 11 03	27	18	25	4	
0104+000	01 04 54.9	00 04 06	27	14	65	...	
0109+182	01 09 08.2	18 16 08	168	82	69	7	
0112+383	01 12 18.2	38 18 59	111	113	52	6	
0113+253	01 13 23.1	25 18 57	73	81	46	5	
0115+253	01 15 46.5	25 19 56	40	27	32	5	
0115+264	01 15 59.1	26 27 30	31	18	20	...	
0117+250	01 17 35.9	25 02 32	62	41	53	6	
0118+234	01 18 33.4	23 27 19	32	29	41	5	
0119+299	01 19 25.5	29 56 53	32	12	37	...	
0120+267	01 20 03.1	26 43 34	50	20	25	...	
0120+289	01 20 07.2	28 58 29	49	29	30	4	
0121+217	01 21 17.8	21 43 00	20	8	32	...	
0121+253	01 21 47.2	25 18 06	77	57	57	6	
0121+384	01 21 51.4	38 29 44	52	23	24	4	
0123+343	01 23 08.8	34 20 50	71	40	36	5	
0123+318	01 23 08.8	31 49 13	10	4	23	...	
0127+266	01 27 47.9	26 36 42	51	24	26	...	*
0133+012	01 33 54.1	01 13 11	33	18	60	8	
0134+266	01 34 28.3	26 38 46	27	18	25	4	
0136+391	01 36 32.7	39 06 00	94	49	49	5	
0139+245	01 39 45.0	24 31 24	744	169	81	8	
0141+126A	01 41 42.4	12 37 39	34	28	74	8	
0141+126B	01 41 46.9	12 38 52	27	23	74	8	
0141+393	01 41 57.8	39 23 30	171	80	80	8	
0149+140	01 49 11.8	14 03 03	14	9	44	6	
0150+362	01 50 51.1	36 16 34	33	17	19	...	
0152+017	01 52 39.7	01 47 18	111	65	51	7	
0159+107	01 59 34.4	10 47 06	103	34	45	6	
0159+022A	01 59 55.5	02 16 56	43	24	63	8	
0200+022B	02 00 02.3	02 16 58	38	22	63	8	
0202+088	02 02 26.5	08 49 14	132	62	62	7	
0204+214	02 04 44.8	21 26 07	9	4	19	...	
0206+245	02 06 02.4	24 35 20	53	35	49	6	
0208+157	02 08 24.8	15 44 15	69	37	46	6	
0210+228	02 10 56.6	22 49 58	41	38	58	6	
0212+010	02 12 25.7	01 01 02	39	24	51	8	
0221+066	02 21 05.0	06 39 42	29	31	33	6	
0232+012	02 32 04.0	01 15 59	27	12	38	...	
0235+034	02 35 19.7	03 29 01	16	17	39	7	
0242+083	02 42 22.7	08 21 24	27	19	80	...	*
0254+364	02 54 00.1	36 25 52	154	73	63	6	
0257+339	02 57 07.9	33 57 30	47	28	20	4	
0308+267	03 08 55.9	26 44 53	23	9	19	...	
0311+147	03 11 33.9	14 42 26	26	13	26	...	
0314+247	03 14 02.7	24 44 31	11	6	44	...	*
0316+090	03 16 12.8	09 04 43	78	51	57	7	
0316+162	03 16 54.0	16 13 45	16	9	32	...	
0317+206	03 17 38.6	20 41 46	68	27	30	5	
0317+222	03 17 46.6	22 13 02	17	5	18	...	
0324+350	03 24 35.9	35 02 47	19	13	22	4	
0324+128A	03 24 38.5	12 53 40	12	6	29	...	
0324+128B	03 24 39.7	12 52 37	28	14	29	...	
0326+024	03 26 14.0	02 25 16	106	68	47	7	
0326+287	03 26 35.3	28 42 56	24	12	116	11	
0331+399	03 31 13.6	39 57 36	19	9	33	...	
0335+191	03 35 19.4	19 06 29	15	7	17	...	*
0336+226A	03 36 03.3	22 36 24	27	16	78	8	
0336+225B	03 36 04.9	22 35 35	105	64	78	8	
0336+268	03 36 31.4	26 52 11	17	6	21	4	
0336+005	03 36 47.4	00 35 19	50	21	74	...	
0338+130	03 38 29.3	13 02 17	39	17	19	...	
0341+266	03 41 17.4	26 40 15	29	12	23	4	
0342+011	03 42 43.6	01 09 50	23	17	48	7	
0342+278	03 42 59.0	27 49 17	141	69	65	7	
0343+388	03 43 12.6	38 53 20	21	27	44	5	
0344+174	03 44 35.6	17 29 31	41	24	71	7	

^aTable 3 is available in its entirety in computer-readable format at <http://cdsweb.u-strasbg.fr/Abstract.html> or <ftp://ftp.astro.psu.edu/pub/edf/rgb.tab3.html> or by contacting the authors.

Table 4. Radio Source Properties: Empty Fields

Name	α (J2000)			δ			Obs	S_5^{tot} (mJy)	ΔS_5^{tot} (mJy)	Notes
	h	m	s	o	l	ll				
0001+083	00	01	19.2	08	20	42.4	d	125	12	
0005+604	00	05	31.3	60	27	00.7	c	21	...	
0012+290	00	12	01.1	29	03	28.1	c	27	...	
0132+027	01	32	02.3	02	46	29.3	c	25	...	
0137+153	01	37	56.9	15	23	54.2	c	25	...	
0140+087	01	40	34.3	08	45	32.4	b	2856	...	*
0205+648	02	05	38.9	64	49	39.4	b	14608	1302	*
0227+335	02	27	27.6	33	34	43.7	b	42	...	
0241+252	02	41	30.9	25	17	21.8	c	18	...	
0247+187	02	47	56.8	18	45	00.7	c	42	5	*
0257+188	02	57	45.7	18	53	25.4	c	20	...	
0258+297	02	58	28.5	29	47	59.6	c	26	...	
0317+415	03	17	28.6	41	31	51.2	b	118	...	*
0353+199	03	53	46.5	19	58	20.3	c	14	...	
0434+152	04	34	39.5	15	12	27.7	c	26	...	
0528+344	05	28	18.0	34	24	57.2	b	355	32	*
0533+210	05	33	55.3	21	04	42.6	b	752	...	*
0535+222	05	35	56.3	22	13	59.5	b	380	...	*
0641+019	06	41	28.0	01	55	53.4	c	26	...	
0641+080	06	41	36.2	08	02	17.5	b	357	...	*
0707+564	07	07	24.7	56	28	06.2	c	19	...	
0722+025	07	22	41.5	02	34	27.8	c	34	...	
0733+644	07	33	49.9	64	29	58.9	c	46	5	
0915+082	09	15	02.9	08	12	53.6	c	30	...	
0915+052	09	15	06.1	05	15	21.2	c	18	...	
0959+384	09	59	44.6	38	29	35.5	c	13	...	
1005+651	10	05	59.5	65	10	29.3	c	13	...	
1015+714	10	15	43.0	71	26	57.8	c	31	...	
1038+535	10	38	46.2	53	30	00.4	b	148	13	
1100+157	11	00	11.2	15	47	10.3	c	19	...	
1107+530	11	07	40.0	53	03	00.4	c	22	...	
1143+021	11	43	19.4	02	11	43.1	e	60	...	
1147+272	11	47	57.9	27	15	05.0	c	24	...	
1149+548	11	49	47.9	54	48	19.1	c	25	...	
1149+023	11	49	48.7	02	21	36.7	e	25	...	
1203+153	12	03	19.7	15	22	42.6	e	26	...	
1204+018	12	04	25.2	01	53	51.0	e	73	...	
1205+425	12	05	22.1	42	31	37.6	c	17	...	
1223+093	12	23	16.8	09	22	45.1	e	24	...	
1231+006	12	31	06.7	00	36	35.3	e	81	...	
1232+123	12	32	04.3	12	23	12.5	c	908	...	*
1241+490	12	41	50.0	49	04	32.9	c	47	...	
1248+075	12	48	15.1	07	31	38.6	c	43	...	
1315+420	13	15	49.2	42	01	52.7	b	83	8	
1413+272	14	13	34.7	27	12	26.3	c	26	...	
1429+361	14	29	37.7	36	07	24.2	c	30	...	
1442+293	14	42	40.2	29	20	39.5	c	34	...	
1546+460	15	46	08.0	46	01	19.6	c	44	...	
1601+254	16	01	12.9	25	26	21.5	c	36	...	
1614+026	16	14	57.4	02	41	46.0	c	36	...	

Name	α (J2000)			δ			Obs	S_5^{tot} (mJy)	ΔS_5^{tot} (mJy)	Notes
	h	m	s	o	l	ll				
1651+254	16	51	47.7	25	24	23.0	c	18	...	
1701+340	17	01	02.0	34	03	59.0	c	24	...	
1703+205	17	03	36.3	20	34	45.5	c	45	...	
1721+304	17	21	29.4	30	28	34.7	c	15	...	
1728+086	17	28	09.7	08	39	23.0	c	24	...	*
1730+509	17	30	09.0	50	57	09.7	c	24	...	
1742+390	17	42	46.9	39	00	20.5	c	35	5	
1748+496	17	48	21.3	49	41	52.4	c	54	...	
1755+741	17	55	21.5	74	09	06.8	c	35	...	
1758+168	17	58	47.1	16	52	25.0	c	50	...	
1801+511	18	01	28.3	51	10	35.0	c	18	...	
1838+049	18	38	44.8	04	55	39.0	c	27	...	
1844+459	18	44	06.7	45	58	04.8	c	15	...	
1852+006	18	52	40.1	00	39	07.9	b	1323	119	*
1859+071	18	59	10.1	07	06	01.4	b	797	...	*
1907+071	19	07	34.5	07	08	21.5	b	4874	437	
2011+382	20	11	53.6	38	15	04.3	b	172	17	
2015+386	20	15	46.1	38	36	08.3	b	376	...	*
2020+001	20	20	33.3	00	11	30.1	c	155	15	
2041+248	20	41	33.0	24	48	45.7	b	319	28	
2044+220	20	44	07.2	22	05	07.8	c	42	...	
2054+008	20	54	18.4	00	49	32.5	c	22	...	
2103+379	21	03	05.5	37	56	29.8	c	42	...	
2114+463	21	14	18.3	46	18	13.3	c	41	5	
2130+032	21	30	44.7	03	14	15.0	b	36	...	
2203+007	22	03	31.5	00	43	54.1	c	27	...	
2206+339	22	06	28.4	33	56	13.9	c	14	...	
2212+589	22	12	53.2	58	59	44.5	b	187	17	*
2243+649	22	43	07.8	64	55	48.4	c	17	...	
2256+356	22	56	44.1	35	41	17.9	b	133	12	
2302+587	23	02	26.7	58	42	41.4	b	507	...	*
2308+000	23	08	50.1	00	01	04.4	c	47	...	
2323+584	23	23	03.9	58	29	45.6	b	820	...	*